Philosophical Magazine Letters,
Vol. 87, No. 8, August 2007, 567–574

Taylor & Francis
Taylor & Francis Group

Downloaded By: [Georgia Technology Library] At: 22:40 12 August 2007

Atomic geometry and energetics of carbon nanotube necking

S. ZHANG*† and T. ZHU‡

†Department of Mechanical Engineering, University Arkansas,
Arkansas 72701, Fayetteville, USA
‡Woodruff School of Mechanical Engineering, Georgia Institute of Technology,
Georgia 30332, Atlanta, USA

(*Received 4 February 2007; accepted in revised form 23 March 2007*)

Molecular mechanics simulations were performed to probe the incipient plastic deformation in carbon nanotubes (CNTs), which involves nucleation of Stone–Wales (SW) defects and spiral glide of 5/7 dislocation dipoles that lead to quantized necking through a stepwise reduction in tube diameter. Quantification of the strain-dependent energetics of dislocation glide reveals that such dislocation motions are energetically favoured at high tensile strain. Pre-existing dislocations critically affect subsequent nucleation and separation of SW defects, as manifested by the competing deformation modes of symmetric versus asymmetric necking. The results provide a quantitative basis for the dislocation dynamics simulations of superplastically deformed CNTs.

1. Introduction

The promising applications of carbon nanotubes (CNTs) as ultra-stiff, high-flexibility fibres in nanocomposites have directed considerable efforts to the study of the mechanics of CNTs both experimentally [1–5] and theoretically [6–24]. At high loads, the deformation of CNTs may take two distinct routes [7]: cleavage brittle fracture [9–11, 13, 15, 21, 22] or plastic flow [7, 8, 11, 12, 16], with active mechanisms mediated by temperature. At low temperatures, brittle fracture via bond breaking prevails and often involves stress-mediated formation of large open-ring structures [9, 10, 15, 21], whereas at elevated temperatures, plastic deformation dominates and proceeds by nucleation and motion of Stone–Wales (SW) defects [8, 11, 12, 16, 19, 23], which can be viewed as a 5/7–7/5 dislocation dipole formed by rotating a C–C bond by 90°. Extensive experiments [1–3] and numerical simulations, ranging from first-principles calculations [6, 9, 10, 12, 13, 15], empirical atomistic simulations [10 11, 17, 21, 22, 24], to Cauchy–Born rule [25] based continuum modelling, have been performed to study the brittle fracture of CNTs. In contrast, the deformation mechanisms of CNTs at high temperatures have received much less attention until the recent discovery of superplastic CNTs [4, 5] in which single-walled carbon nanotube (SWCNT) underwent 280% elongation and 15-fold radial reduction with marked kink formation at about 2000°C. Whereas in-situ experiments have

*Corresponding author. Email: szhang1@uark.edu

Philosophical Magazine Letters
ISSN 0950-0839 print/ISSN 1362-3036 online © 2007 Taylor & Francis
http://www.tandf.co.uk/journals
DOI: 10.1080/09500830701370799

Downloaded By: [Georgia Technology Library] At: 22:40 12 August 2007

demonstrated that such a superplastic deformation results from post-yield plastic flow in the form of glide and climb of dislocations [4], quantitative atomistic modelling of the necking geometry and the energetics of dislocations in CNTs has not yet been performed; such a study is critically needed for a fundamental understanding of deformation physics of plastic CNTs.

For 5/7 dislocations in a CNT clamped at the ends, the total energy of the system consists of the elastic energy of the otherwise perfect CNT, the self-energy of dislocations, the dislocation–dislocation interaction energy, and the dislocation–boundary interaction energy (equivalent to interaction energy of image dislocations) [26]. Due to the complex interaction of image dislocations in a cylindrical tube of finite length, analytical treatment of dislocation motion and patterning in CNTs is not straightforward. In this letter, molecular mechanics simulations are employed to probe the strain-dependent energetics of dislocations at a series of local equilibrium states, as well as their effects on the incipient plastic deformation that leads to CNT necking. Through this research, we reveal some new features associated with dislocation interactions on the cylindrically curved surface of CNTs, and examine their influence on CNT necking.

2. Methodology

A CNT can be formed by rolling a graphene sheet in a specified direction. For a CNT indexed by a pair of integers (n, m), its rolling direction (or the circumferential direction) is denoted by $\mathbf{c} = n\mathbf{a} + m\mathbf{b}$, where $\mathbf{a}$ and $\mathbf{b}$ are two base vectors, as shown in figure 1a. Owing to the hexagonal symmetry of the graphene structure, an SW defect can be nucleated from a pristine CNT by a 90° rotation of one of three possible C–C bonds. With the same base vectors [$\mathbf{a}$,$\mathbf{b}$], these three bonds, denoted by a_1, a_2, and a_3,

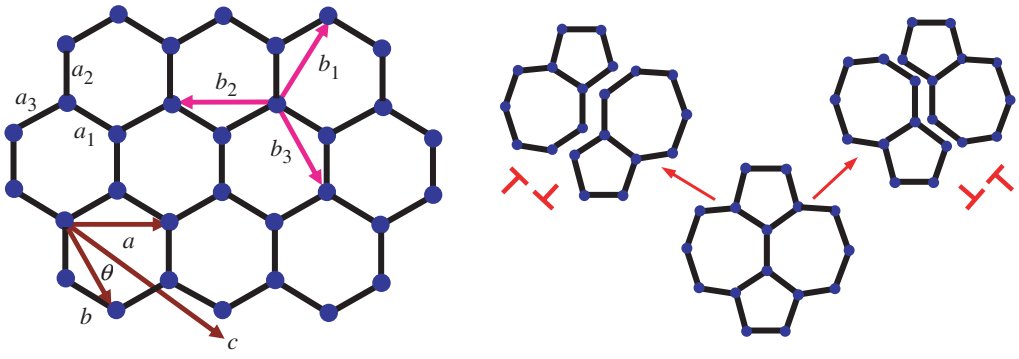

Figure 1. Schematics of SW defect formation and dislocation glide in CNTs. (a) A SW defect can form by a 90° rotation of one of the three bonds, a_1, a_2 and a_3; a dislocation can glide along three possible $\langle \bar{1}\ \bar{1}\ 2\ 0 \rangle$ directions with the corresponding Burgers vectors b_1, b_2 and b_3. The circumference c and the chiral angle θ can be characterized by the base vectors [$\mathbf{a}$,$\mathbf{b}$], as given in the text. (b) An SW defect can be viewed as a 5/7–7/5 dislocation dipole, which has two distinct separation directions.

Downloaded By: [Georgia Technology Library] At: 22:40 12 August 2007

are indexed by (1, 1), (1, 0), and (0, 1), respectively, as shown in figure 1a. For each 5/7–7/5 dislocation dipole, there are two geometrically equivalent gliding directions (i.e. the $\langle \bar{1}\ \bar{1}\ 2\ 0 \rangle$ directions of the closest zigzag atomic packing corresponding to the three Burgers vectors shown in figure 1a) oriented at $\pi/3$ to each other (figure 1b). Note that while all of those nucleation mechanisms and gliding directions may possibly be activated under elevated temperatures and tensile strains, previous analysis [16] has shown that the dislocation dipole nucleated via the rotation of bond a_1 results in the highest elastic strain energy release; the thermodynamic driving force for the subsequent separation of the dislocation dipole is maximized along $\pm(0,1)$ directions. Thus, unless otherwise mentioned, our studies of energetics of CNT necking will be focused on this combined mode of energetically favourable nucleation and glide of 5/7 dislocations.

In our molecular mechanics simulations, the second-generation Brenner potential [27] is adopted to characterize the C–C covalent binding interactions. A (10,10) armchair tube of about 120 Å in length, capped with hydrogen atoms, is chosen as the simulation model. The tube is first relaxed without any constraint using a limited memory BFGS geometry optimization algorithm [28]. The fully relaxed pristine tube is taken as a reference state for the characterization of the energetics of SW nucleation and subsequent glide of 5/7 dislocations.

An SW defect is introduced by a 90° rotation of a (1, 1) bond at the centre of the tube. The system is relaxed with the boundary constraints, i.e. a ring of C atoms adjacent to the capping hydrogens at each end of the CNT are fixed. The dislocation dipole is separated by alternatively gliding along the (0, 1) and (0, –1) directions. Each gliding step results in an increase of separation by one hexagon between the 5/7 and 7/5 dislocations with a separation distance of $\sqrt{3}d\sin(\pi/3-\theta)$ along the tube axis, where d and θ are, respectively, the lattice constant and the chiral angle of the tube. At each gliding step, the configuration is relaxed to a local equilibrium state under the fixed-end constraints.We have also studied the formation of the second SW defect from the same nucleation site as the first SW defect. In the course of the formation and separation of the second dislocation pair, the pre-existing dislocations may move towards the fixed ends due to repulsion from the second dislocation pair. This complication is not studied in detail. Rather, we assume that the repulsion from the fixed boundary is sufficiently large such that the first pair of dislocations is rendered immobile. With this assumption, we can simplify the subsequent analysis of the effects of pre-existing dislocations on the formation of the second SW defect at different nucleation sites.

3. Results and discussion

Figure 2 shows the strain-dependent energy variation associated with the spiral glide of dislocation pairs in a (10,10) tube, which involves the nucleation of two SW defects in sequence, leading to the formation of a (10,10)/(10,8)/(10,10) heterojunction, with atomic structures shown in figures 3a–3e. In figure 2, the x-axis denotes the separation of the 5/7 and 7/5 dislocations; the integer coordinate specifies the number of hexagons between the dislocation pair in the $\langle \bar{1}\ \bar{1}\ 2\ 0 \rangle$ glide

Downloaded By: [Georgia Technology Library] At: 22:40 12 August 2007

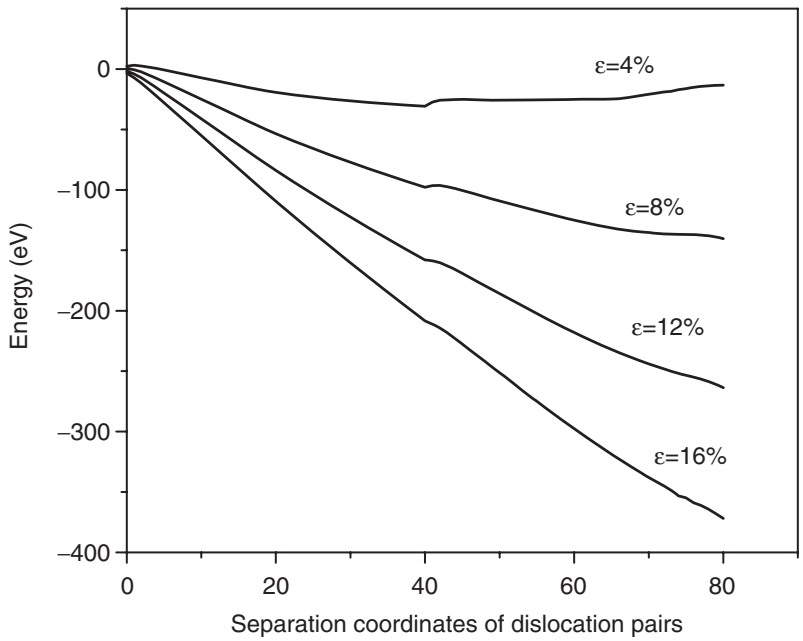

Figure 2. Energetics of formation and subsequent separation of SW defects at different strains, ε. The x-axis specifies the number of hexagons between the dislocation pair in the $\langle\bar{1}\ \bar{1}\ 2\ 0\rangle$ gliding direction, and one helical cycle corresponds to a change in the coordinate by 20. The first SW defect nucleates at the separation coordinate 0 and the second one at the coordinate 41. The pristine (10,10) tube at the same strain is referenced as the zero-energy state.

direction, and coordinate 40 represents the state with the dislocation pair separated by two helical cycles of the tube. The segment of the tube between the 5/7 and 7/5 dislocations changes to a (10,9) tube with a stepwise reduction in diameter, producing a (10,10)/(10,9)/(10,10) heterojunction separated by two 'quantized' necks, as shown in figure 3b.

In figure 2, the coordinates from 41 to 80 correspond to necking from a (10,9) tube to a (10,8) tube, beginning with the nucleation of the second SW defect at the centre of the tube. Notice that here we study the situation where the second SW defect forms on the same side of the tube as the first SW defect (see figure 3b). The second 5/7–7/5 pair is subsequently separated along the same gliding plane as the first pair. As the newly formed 5/7 dislocations approach those of the first SW defect, the heterojunction becomes (10,10)/(10,8)/(10,10) separated by two closely spaced 7/5 dislocations at each junction (see figure 3c).

The energy difference between the two consecutive states is the thermodynamic driving force for dislocation glide. At each applied strain ε and for a given pair of 5/7–7/5 dislocations, there exists a global equilibrium corresponding to the most energetically favourable separation between the two dislocations. With increasing strain, the global equilibrium is shifted to larger separation, as shown in figure 2.

To examine the influence of the pre-existing dislocations on the subsequent formation of SW defects, we have further studied the formation and separation of the second SW defects from other nucleation sites. Specifically, we consider a site at the centre of the tube, but opposite to the site where the first SW defect nucleates (see figure 3d). The subsequent separation of this 5/7–7/5 dislocation pair

Downloaded By: [Georgia Technology Library] At: 22:40 12 August 2007

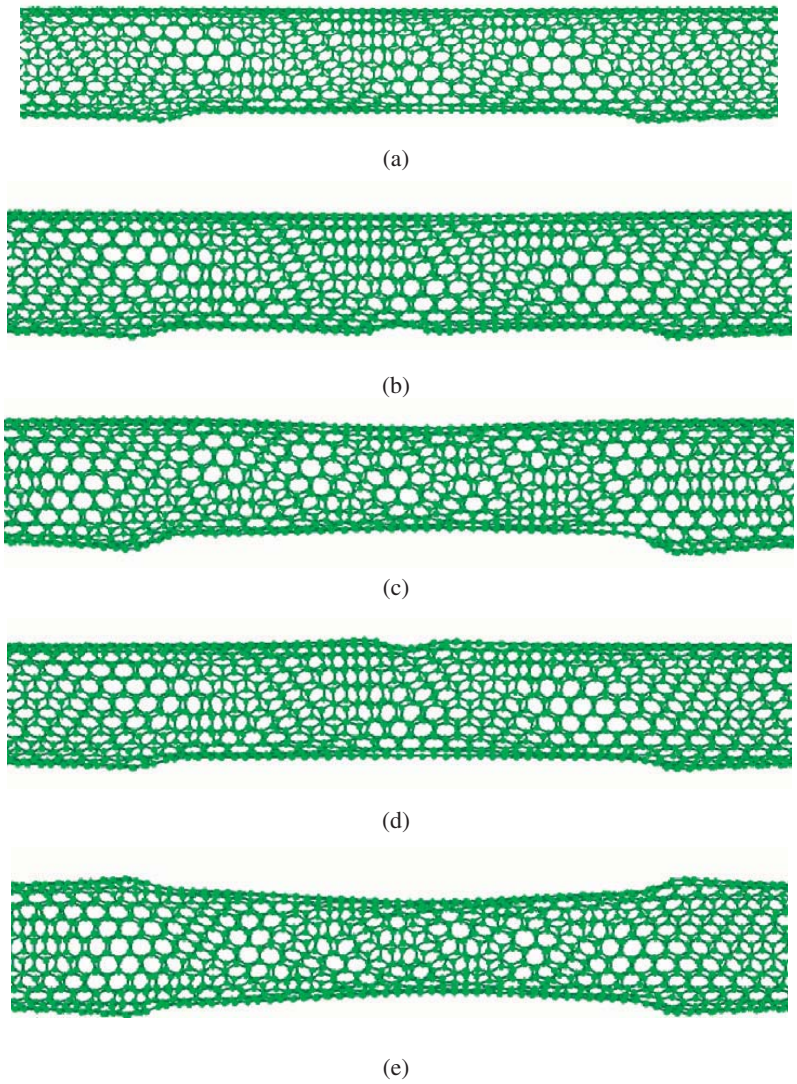

Figure 3. Stepwise necking of a (10,10) tube into a (10,10)/(10,8)/(10,10) heterojunction. (a) The first-step necking (10,10) → (10,9) involves the nucleation and separation of a pair of 5/7–7/5 dislocations. (b) The second SW defect nucleates from the same site as the first one, a dent appears at the nucleation site; (c) the separation of this SW defect leads to asymmetric necking. (d) The second SW defect nucleates from the site opposite to the first one; a dent appears at the nucleation site; (e) the separation of this SW defect causes symmetric necking.

leads to *symmetric* necking, as shown in figure 3e. This process is in contrast to the previous case where two SW defects nucleate sequentially from the same site (figure 3b), causing *asymmetric* necking, as shown in figure 3c.

Figure 4a shows the energy difference, ΔE, for the above two processes that yield either asymmetric or symmetric necking. Here $\Delta E = E_a - E_s$, where E_a and E_s are the energies corresponding to the asymmetric and symmetric necking, respectively. It is seen that for the formation and initial separation of the second dislocation pair, asymmetric necking is energetically more favourable than symmetric necking ($\Delta E < 0$). In other words, the site spatially close to the pre-existing dislocations is favoured compared with the site away from pre-existing dislocations. However, when

Downloaded By: [Georgia Technology Library] At: 22:40 12 August 2007

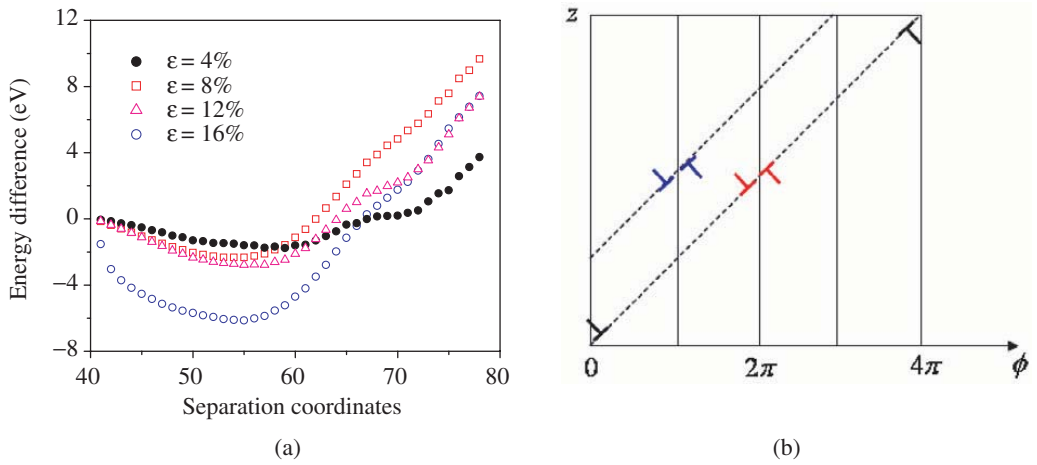

(a) (b)

Figure 4. (a) The difference in energetics of forming and separating the second SW defect from the site same as the first one and that opposite to the first one, with a pre-existing dislocation pair in the tube. (b) Schematics of the flattened surface of a cylindrical CNT, showing the arrangement of the SW defects. $\phi = 0$ and 4π: the dislocations of the first nucleated SW defect; $\phi = 2\pi$: SW defect nucleated at the same site as the first one; $\phi = \pi$: SW defect formed at the site opposite to the first one. One spiral cycle of glide corresponds to a change in the azimuthal angle ϕ by 2π; z denotes the coordinate along the tube.

the separation of the second 5/7–7/5 pair is increased, this trend gradually reverses ($\Delta E > 0$) as indicated by the minimum of each curve in figure 4a.

The energy difference shown in figure 4a can be understood in terms of dislocation interaction on a cylindrical surface. Note that in considering the long range elastic interaction, the distance between dislocations on the curved surface of the tube should be the spiral separations rather than the spatial distances, as indicated by the dashed lines in figure 4b, where the curved surface of the cylindrical tube has been flattened out. It is evident from figure 4b that the two sites of forming the second SW defects (which are occupied by the blue and red pairs of 5/7–7/5 dislocations, respectively) are subjected to different elastic constraints from the pre-existing 5/7–7/5 dislocations (the dislocation pair at $\phi = 0$) due to their differences in distance to the pair at $\phi = 0$. To simplify the analysis, here we ignore the elastic interaction arising from image dislocations in both axial and azimuthal directions of the cylindrical tube. According to figure 4b, the formation of the pair at $\phi = \pi$ should be more difficult than that of the pair at $\phi = 2\pi$, because the former is spirally closer to the pre-existing dislocations and thus subjected to stronger elastic constraints. In contrast, when separations are large, the pair at $\phi = 2\pi$ experiences stronger repulsion from pre-existing dislocations than does the pair at $\phi = \pi$, because of the constraint of the pre-existing dislocations within the same glide plane, thus causing the minimum of each curve in figure 4a.

4. Conclusions

In summary, our molecular mechanics simulations quantitatively characterize the atomic geometry and strain-dependent energetics of formation and separation of SW

Downloaded By: [Georgia Technology Library] At: 22:40 12 August 2007

defects in CNTs; these processes can lead to quantized necking through a stepwise reduction in the tube diameter. Specifically, we have identified two competing modes of atomic-scale necking, i.e. symmetric versus asymmetric neck formation and propagation in CNTs. We have further studied the mechanics governing this competing process based on the elastic interactions between dislocations on a cylindrical surface of curved CNTs. These results can guide the formulation of continuum constitutive model, and also provide a quantitative basis for the dislocation dynamics simulations of superplastically deformed CNT.

We conclude by commenting that the present study focuses on the thermodynamic driving forces of the formation and glide of dislocations. For a complete description of dislocation activities in CNTs, it is also necessary to evaluate the activation energy barriers of dislocation nucleation and motion that control the kinetic rate of plastic flow. Also note that the plastic deformation in CNTs may proceed by dislocation climb [4]. Such a process will compete against dislocation spiral glide to sustain the plastic flow of CNTs at high temperatures. Activation energy barriers between consecutive slip steps of 5/7 dislocations in bent CNTs have recently been calculated by Mori *et al.* [29], where only one dislocation dipole was considered. In order to obtain a full understanding of the large plastic flow in CNTs, work is currently underway to compute the activation energy barriers of sequential dislocation nucleation and motion (both slip and climb) in CNTs using the atomic configurations obtained from the present study.

Acknowledgements

We thank Professor Ted Belytschko for helpful discussions. S. Zhang acknowledges the grant support from the National Science Foundation grant under award No. 0600661 (Clark V. Cooper, Program Manager). T. Zhu acknowledges the support from AFOSR/MURI Grant F49620-02-1-0382.

References

[1] B.G. Demczyk, Y.M. Wang, J. Cumings, *et al.*, Mater. Sci. Eng. A **334** 173 (2002).
[2] D.A. Walters, L.M. Ericson, M.J. Casavant, *et al.*, Appl. Phys. Lett. **74** 3803 (1999).
[3] M.F. Yu, O. Lourie, M.J. Dyer, K. Moloni, *et al.*, Science **287** 637 (2000).
[4] J.Y. Huang, S. Chen, Z.F. Ren, *et al.*, Phys. Rev. Lett. **97** 075501 (2006).
[5] J.Y. Huang, S. Chen, Z.Q. Wang, *et al.*, Nature **439** 281 (2006).
[6] T. Dumitrica, T. Belytschko and B.I. Yakobson, J. chem. Phys. **118** 9485 (2003).
[7] T. Dumitrica, M. Hua and B.I. Yakobson, Proc. Natn. Acad. Sci. U.S.A. **103** 6105 (2006).
[8] T. Dumitrica and B.I. Yakobson, Appl. Phys. Lett. **84** 2775 (2004).
[9] R. Khare, S.L. Mielke, J.T. Paci, *et al.*, Phys. Rev. B **75** 075412 (2007).
[10] S.L. Mielke, D. Troya, S. Zhang, *et al.*, Chem. Phys. Lett. **390** 413 (2004).
[11] M.B. Nardelli, B.I. Yakobson and J. Bernholc, Phys. Rev. Lett. **81** 4656 (1998).
[12] M.B. Nardelli, B.I. Yakobson and J. Bernholc, Phys. Rev. B **57** R4277 (1998).
[13] S. Ogata and Y. Shibutani, Phys. Rev. B **68** 165409 (2003).
[14] G.G. Samsonidze, G.G. Samsonidze and B.I. Yakobson, Phys. Rev. Lett. **88** 065501 (2002).

Downloaded By: [Georgia Technology Library] At: 22:40 12 August 2007

[15] D. Troya, S.L. Mielke and G.C. Schatz, Chem. Phys. Lett. **382** 133 (2003).
[16] B.I. Yakobson, Appl. Phys. Lett. **72** 918 (1998).
[17] B.I. Yakobson, M.P. Campbell, C.J. Brabec, *et al.*, Comput. Mater. Sci. **8** 341 (1997).
[18] B.I. Yakobson and L.S. Couchman, J. Nanoparticle Res. **8** 105 (2006).
[19] B.I. Yakobson, G. Samsonidze and G.G. Samsonidze, Carbon **38** 1675 (2000).
[20] S.L. Zhang, R. Khare, T. Belytschko, *et al.*, Phys. Rev. B **73** 075423 (2006).
[21] S.L. Zhang, S.L. Mielke, R. Khare, *et al.*, Phys. Rev. B **71** 115403 (2005).
[22] T. Belytschko, S.P. Xiao, G.C. Schatz, *et al.*, Phys. Rev. B **65** 235430 (2002).
[23] G.G. Samsonidze, G.G. Samsonidze and B.I. Yakobson, Comput. Mater. Sci. **23** 62 (2002).
[24] C.Y. Wei, K. Cho and D. Srivastava, Appl. Phys. Lett. **82** 2512 (2003).
[25] M. Arroyo and T. Belytschko, Int. J. Numer. Meth. Eng. **59** 419 (2004).
[26] Z.L. Li, P. Dharap, P. Sharma, *et al.*, J. Appl. Phys. **97** 074303 (2005).
[27] D.W. Brenner, O.A. Shenderova, J.A. Harrison, *et al.*, J. Phys. Condensed Mat. **14** 783 (2002).
[28] R.H. Byrd, P. Lu and J. Nocedal, SIAM J. Sci. Comput. **16** 1190 (1995).
[29] H. Mori, S. Ogata, J. Li, *et al.*, Phys. Rev. B **74** 165418 (2006).